Inorg. Chem. **2006**, *45*, 7408–7416

Localized and Delocalized Chemical Bonding in the Compounds $CaNiGe_2$, $SrNiGe_2$, and $SrNiSn_2$

Viktor Hlukhyy, Steffen Eck, and Thomas F. Fässler*

Department Chemie, Technische Universität München, Lichtenbergstrasse 4, D-85747 Garching, Germany

Received April 11, 2006

The new compounds $CaNiGe_2$, $SrNiGe_2$ and $SrNiSn_2$ have been synthesized from the elements by arc melting techniques with subsequent annealing of the sample at 1270 K, and their structures have been determined by single-crystal X-ray diffraction methods. They crystallize in the $CeNiSi_2$ structure (space group *Cmcm*). For $CaNiGe_2$: $a = 4.2213(7)$ Å, $b = 17.375(4)$ Å, $c = 4.0514(7)$ Å, $R_1 = 0.033$ (all data); for $SrNiGe_2$: $a = 4.429(1)$ Å, $b = 17.420(4)$ Å, $c = 4.200(1)$ Å, $R_1 = 0.041$ (all data); and for $SrNiSn_2$: $a = 4.5924(7)$ Å, $b = 18.710(3)$ Å, $c = 4.5228(6)$ Å, $R_1 = 0.021$ (all data). The main structural motifs are two-dimensionally condensed Ni-centered Ge_5 or Sn_5 square pyramids. The crystal chemistry and chemical bonding are discussed. Analyses of the electronic structures of $CaNiGe_2$, $SrNiGe_2$, and $SrNiSn_2$, with the help of the electron localization function (ELF), indicate the coexistence of localized covalent and delocalized bonding between the metal atoms involved.

Introduction

The coexistence of localized and delocalized chemical bonding between atoms of same type within a single compound is a fascinating phenomenon in intermetallic chemistry that drastically influences the physical properties, such as thermoelectricity or superconductivity.

In binary alkali- or alkaline-earth metal stannides, the bonding characteristic can readily be tuned by changing the stoichiometry of the components. In the Na−Sn phase system, the transition from localized to delocalized bonding has been demonstrated.[1] In agreement with the concept by Zintl, Klemm, and Busmann (ZKB),[2] the 1:1 phase NaSn contains tetrahedral Sn_4^{4-} units with localized two-center−two-electrons bonds. An increase in the Sn content leads to the Zintl phases Na_7Sn_{12} and $NaSn_2$, and finally to $NaSn_5$, in which quadratic networks of Sn atoms with delocalized bonds and structural motifs that contain localized Sn−Sn bonds are present at the same time. A similar trend holds for the Ba−Sn system, because the 1:1 phase BaSn is a Zintl phase with two-coordinate Sn atoms in the form of zig-zag chains, whereas in $BaSn_3$, the Zintl concept can still be recognized in the formally electron-precise Sn_3^{2-} anions; however, the anion can also be described as a three-membered ring with a two-electron π-system. Strong interactions between these π-systems of coplanar anionic units within the one-dimensional chain $^1_\infty[Sn_3^{2-}]$ lead to a metallic electronic band character.[3] $BaSn_3$, as well as the Sn-richest phase $BaSn_5$, are superconducting. The latter adapts an AlB_2-type structure with high coordination numbers for Sn, which is typical for intermetallic compounds.[4] Recently, the coexistence of localized and delocalized bonding between Sn atoms has also been described for $SrSn_4$ and correlated with the superconducting properties of this compound.[5]

In the course of our studies on Ge- and Sn-rich alloys with transition metals as additional components, short Ge−Ge and Sn−Sn contacts have been detected in $MgCo_6Ge_6$ and $Mg_2Co_3Sn_{10}$, which are indicative for homoatomic localized bonds,[6] and similar homoatomic bonds can also be expected in the compounds $CeNiSi_2$, $YIrGe_2$, and $LuNiSn_2$. Among the large number of ternary stannides and germanides, there are very many phases that contain a rare-earth metal (RE) and a transition metal (T), and many of them have the

* To whom correspondence should be addressed. E-mail: thomas.faessler@lrz.tu-muenchen.de.

(1) Fässler, T. F. *Z. Anorg. Allg. Chem.* **2006**, *632*, 1125.
(2) (a) Zintl, E. *Angew. Chem.* **1939**, *52*, 1. (b) Klemm, W. *Proc. Chem. Soc., London* **1958**, 329.
(3) Fässler, T. F.; Kronseder, C. *Angew. Chem., Int. Ed. Engl.* **1997**, *36*, 2683.
(4) Fässler, T. F.; Hoffmann, S.; Kronseder, C. *Z. Anorg. Allg. Chem.* **2001**, *627* (11), 2486.
(5) Hoffmann, S.; Fässler, T. F. *Inorg. Chem.* **2003**, *42* (26), 8748.
(6) (a) Gieck, C.; Schreyer, M.; Fässler, T. F.; Cavet, S.; Claus, P. *Chem.—Eur. J.* **2006**, *12*, 1924. (b) Schreyer, M.; Kraus, G.; Fässler, T. F. *Z. Anorg. Allg. Chem.* **2004**, *630*, 2520.

10.1021/ic060613y CCC: $33.50
Published on Web 08/11/2006

Table 1. Crystal Data and Structure Refinement of $CaNiGe_2$, $SrNiGe_2$, and $SrNiSn_2$

parameter	value		
	$CaNiGe_2$	$SrNiGe_2$	$SrNiSn_2$
formula weight	243.97 g/mol	291.51 g/mol	383.73 g/mol
temperature, T	293(2) K	293(2) K	293(2) K
space group	*Cmcm*	*Cmcm*	*Cmcm*
unit-cell dimensions[a]			
a	4.2213(7) Å	4.429(1) Å	4.5924(7) Å
b	17.375(4) Å	17.420(4) Å	18.710(3) Å
c	4.0514(7) Å	4.200(1) Å	4.5228(6) Å
volume, V	297.2(1) Å^3	324.0(2) Å^3	388.6(1) Å^3
Z	4	4	4
calculated density	5.453 g/cm^3	5.977 g/cm^3	6.553 g/cm^3
diffractometer	Oxford Xcalibur3	Stoe IPDS-IIT	Stoe IPDS-IIT
absorption coefficient	27.8 mm^{-1}	40.2 mm^{-1}	30.8 mm^{-1}
$F(000)$	448	520	663
crystal size	0.20 mm × 0.10 mm × 0.10 mm	0.11 mm × 0.05 mm × 0.05 mm	0.12 mm × 0.10 mm × 0.10 mm
θ range for data collection	4.69−27.66°	4.68−27.37°	4.36−27.48°
index ranges	$-4 \le h \le 5$; ± 22; $-4 \le l \le 5$	± 5; ± 22; ± 5	$-4 \le h \le 5$; ± 22; $-5 \le l \le 4$
reflections collected	1730	2409	2043
independent reflections	222 ($R_{int} = 0.029$)	233 ($R_{int} = 0.099$)	278 ($R_{int} = 0.091$)
reflections with $I \ge 2\sigma(I)$	203 ($R_{sigma} = 0.014$)	219 ($R_{sigma} = 0.037$)	272 ($R_{sigma} = 0.033$)
data/parameters	222/18	233/19	278/21
GOF on F^2	1.210	1.208	1.226
final R indices [$I \ge 2\sigma(I)$]	$R_1 = 0.031$	$R_1 = 0.038$	$R_1 = 0.020$
	$wR_2 = 0.079$	$wR_2 = 0.083$	$wR_2 = 0.042$
R indices (all data)	$R_1 = 0.033$	$R_1 = 0.041$	$R_1 = 0.021$
	$wR_2 = 0.080$	$wR_2 = 0.087$	$wR_2 = 0.043$
extinction coefficient	0.0034(9)	0.0072(13)	0.0029(2)
largest diffraction peak and hole	2.01 and −1.97 e/Å^3	1.22 and −1.29 e/Å^3	0.93 and −0.84 e/Å^3

[a] Powder data.

composition (RE)TX_2 (where X = Ge, Sn). For T = Ni, RE = lanthanide metal, and X = Ge, Sn, these compounds adopt either the $CeNiSi_2$ structure (RE = La−Nd, Sm for X = Sn; RE = La−Nd, Sm−Er for X = Ge), or crystallize in the $YIrGe_2$ (RE = Dy−Yb, Lu for X = Ge) and $LuNiSn_2$ (RE = Y, Gd−Tm, X = Sn) lattices.[7−14]

Some of the germanides of the $CeNiSi_2$ type crystallize with the ideal composition 1:1:2,[15] whereas most of the germanides and stannides form a range of solid solutions (RE)$Ni_{1-x}Ge_2$ and (RE)$Ni_{1-x}Sn_2$ characterized by different degrees of Ni deficiency.[8,10,11] Furthermore, some stannides reveal defects in the tin positions, which leads to (RE)$Ni_{1-x}Sn_{2-y}$ phases.[8] However, only a few alkaline-earth metal (AE) stannides and germanides of the composition 1:1:2 have been reported. The compounds $CaTSn_2$ (where T = Rh, Pd, Ir) crystallize in the $MgCuAl_2$ structure,[16] whereas $BaCuSn_2$ and $SrCuSn_2$ adopt the $CeNiSi_2$ structure.[17,18] $SrAuSn_2$ is described as a commensurately modulated structure of the $CeNiSi_2$ type.[19] In the AE−Ni−Ge,Sn systems, the ternary compounds $SrNi_2Ge_2$,[20] $SrNiGe_3$,[21] $BaNiSn_3$,[22] $Ba_4Ni_3Ge_{20}$,[23] $MgNi_2Sn$,[24] $Mg_{74.5}Ni_{14.5}Sn_{11}$,[25,26] $Mg_{2-x}NiSn_x$,[27] $Mg_6Ni_{16}Ge_7$,[28] $Ca_7Ni_4Sn_{13}$,[29] $CaNi_4Sn_2$,[30] $CaNi_2Ge_2$,[20] $CaNiGe_3$,[21] $SrNiSn_3$,[22] and $SrNi_4Sn_2$ [30] have been described.

We started a systematic investigation of phases that consist of alkaline-earth metals, nickel, and germanium or tin, with two- or three-dimensionally infinite Ge or Sn and Ni−Ge or Ni−Sn polyanions as their main structural motifs. Here, we report on the synthesis and the structure of the novel

(7) Bodak, O. I.; Gladyshevskii, E. I. *Kristallografiya* **1969**, *14* (6), 990.
(8) Skolozdra, R. V. Stannides of Rare-Earth and Transition Metals. In *Handbook on the Physics and Chemistry of Rare Earths*, Vol. 14; Gschneidner, K. A., Jr., Eyring, L., Eds.; Elsevier: Amsterdam 1997; Chapter 164.
(9) Schobinger-Papamantellos, P.; Rodriguez-Carvajal, J.; Prokes, K.; Buschow, K. H. J. *J. Phys.: Condens. Matter* **1996**, *8*, 8635.
(10) Francois, M.; Venturini, G.; Malaman, B.; Roques, B. *J. Less-Common Met.* **1990**, *160*, 197.
(11) Venturini, G.; Francois, M.; Malaman, B.; Roques, B. *J. Less-Common Met.* **1990**, *160*, 215.
(12) Salamakha, P.; Sologub, O.; Yakinthos, J. K.; Routsi, Ch. D. *J. Alloys Compd.* **1998,** *267*, 192.
(13) Proserpio, D. M.; Chacon, G.; Zheng, Ch. *Chem. Mater.* **1998,** *10*, 1286.
(14) Salvador, J. R.; Gour, J. R.; Bilc, D.; Mahanti, S. D.; Kanatzidis, M. G. *Inorg. Chem.* **2004**, *43*, 1403.
(15) Villars, P.; Calvert, L. D. *Pearson's Handbook of Crystallographic Data for Intermetallic Phases*, Second Edition; American Society for Metals: Materials Park, OH, 1991. (Also in Desk Edition, 1997.)
(16) Hoffmann, R.-D.; Kussmann, D.; Rodewald, U. Ch.; Pöttgen, R.; Rosenhahn, C.; Mosel, B. D. *Z. Naturforsch.* **1999**, *54b*, 709.
(17) Dörrscheidt, W.; Savelsberg, G.; Stöhr, J.; Schäfer, H. *J. Less-Common Met.* **1982**, *83*, 269.
(18) May, N.; Schaefer, H. *Z. Naturforsch.* **1974**, *29b*, 20.
(19) Esmailzadeh, S.; Hoffmann, R.; Pöttgen, R. *Z. Naturforsch.* **2004**, *59b*, 1451.
(20) Bodak, O. I.; Gladyshevskii, E. I. *Dopov. Akad. Nauk. Ukr. RSR* **1968**, *30* (10), 944.
(21) Hlukhyy, V.; Fässler, T. F. GDCh-Jahrestagung, Düsseldorf, Germany, 2005; Poster abstract Mat-020.
(22) Dörrscheidt, W.; Schäfer, H. *J. Less-Common Met.* **1978**, *58*, 209.
(23) Cordier, G.; Woll, P. *J. Less-Common Met.* **1991**, *169* (2), 291.
(24) Rahlfs, P. *Metallwirtsch., Metallwiss., Metalltech.* **1937**, *16*, 640.
(25) Boudard, M.; Doisneau, B.; Audebert, F. *J. Alloys Compd.* **2004**, *370*, 169.
(26) Boudard, M.; Bordet, P.; Vincent, H.; Audebert, F. *J. Alloys Compd.* **2004**, *372*, 121.
(27) Hlukhyy, V.; Rodewald, U. Ch.; Pöttgen, R. *Z. Anorg. Allg. Chem.* **2005**, *631* (15), 2997.
(28) Markiv, V. Y.; Teslyuk, M. Y.; Gladyshevskii, E. I. *Dopov. Akad. Nauk. Ukr. RSR* **1961**, *7*, 914.
(29) Vennos, D. A.; Badding, M. E.; DiSalvo, F. J. *J. Less-Common Met.* **1991**, *175*, 339.
(30) Hlukhyy, V.; Fässler T. F. 7th International Conference on Crystal Chemistry of Intermetallic Compounds, Lviv, Ukraine, 2005; Poster abstract P44.

Table 2. Atomic and Isotropic Displacement Parameters of the Compounds $CaNiGe_2$, $SrNiGe_2$, and $SrNiSn_2$

atom	Wyckoff position	occupancy (%)	*x*	*y*	*z*	U_{eq} ($\times 10^3$ Å^2)
			$CaNiGe_2$			
Ca	4c	100	0	0.10834(9)	$^1/_4$	12(1)
Ni	4c	100	0	0.32334(7)	$^1/_4$	12(1)
Ge1	4c	100	0	0.45807(6)	$^1/_4$	13(1)
Ge2	4c	100	0	0.75094(6)	$^1/_4$	13(1)
			$SrNiGe_2$			
Sr	4c	100	0	0.10761(7)	$^1/_4$	17(1)
Ni	4c	100	0	0.3199(1)	$^1/_4$	17(1)
Ge1	4c	100	0	0.45782(8)	$^1/_4$	20(1)
Ge2	4c	100	0	0.75045(8)	$^1/_4$	21(1)
			$SrNiSn_2$			
Sr	4c	100	0	0.10955(4)	$^1/_4$	14(1)
Ni	4c	98.1(4)	0	0.31940(6)	$^1/_4$	14(1)
Sn1	4c	100	0	0.45395(3)	$^1/_4$	16(1)
Sn2	4c	100	0	0.74942(3)	$^1/_4$	12(1)

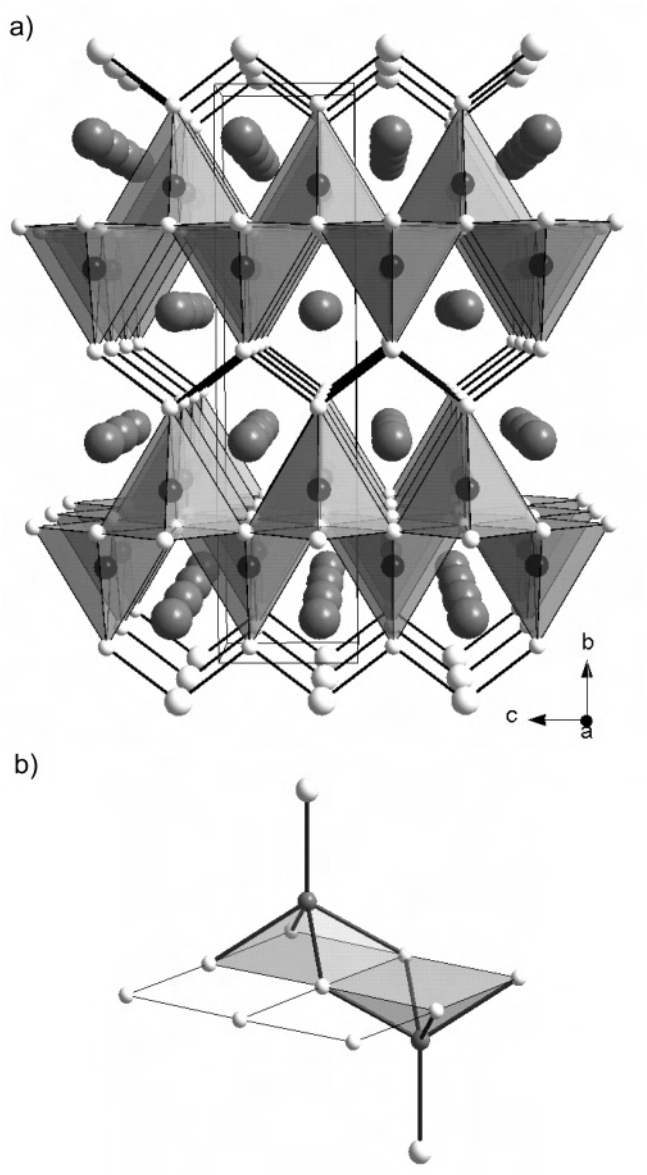

Figure 1. Schematics of the structure of $SrNiSn_2$. Sr atoms are drawn as large gray spheres, whereas Sn and Ni atoms in white and small dark gray, respectively: (a) three-dimensional network of condensed distorted Ni-centered Sn_5 square pyramids and Sn zig-zag chains, and (b) detail of the structure including bonding contacts in the vicinity of the quadratic network of Sn2 atoms.

Table 3. Interatomic Distances in $CaNiGe_2$, $SrNiGe_2$, and $SrNiSn_2$

	interatomic distance (Å)[a]		
	$CaNiGe_2$	$SrNiGe_2$	$SrNiSn_2$
	For Ca(Sr)		
4 Ge1 (Sn1)	3.145	3.257	3.435
4 Ni	3.157	3.302	3.486
2 Ge2 (Sn2)	3.175	3.244	3.475
2 Ge2 (Sn2)	3.255	3.331	3.482
2 Ge1 (Sn1)	3.357	3.422	3.708
1 Ni	3.736	3.699	3.926
	For Ni		
1 Ge1 (Sn1)	2.341	2.402	2.517
2 Ge2 (Sn2)	2.402	2.432	2.602
2 Ge2 (Sn2)	2.457	2.524	2.643
4 Ca(Sr)	3.157	3.302	3.486
1 Ca(Sr)	3.736	3.699	3.926
	For Ge1(Sn1)		
1 Ni	2.341	2.402	2.517
2 Ge1 (Sn1)	2.495	2.563	2.843
4 Ca (Sr)	3.145	3.257	3.435
2 Ca (Sr)	3.357	3.422	3.708
2 Ge2 (Sn2)	4.405	4.192	4.426
	For Ge2(Sn2)		
2 Ni	2.402	2.432	2.602
2 Ni	2.457	2.524	2.643
4 Ge2 (Sn2)	2.926	3.052	3.223
2 Ca (Sr)	3.175	3.244	3.475
2 Ca (Sr)	3.255	3.331	3.482
2 Ge1 (Sn1)	4.051	4.192	4.426

[a] Standard deviations are all ≤0.002 Å.

phases $CaNiGe_2$, $SrNiGe_2$, and $SrNiSn_2$. They crystallize in the $CeNiSi_2$ structure in which short contacts between the atoms of the majority component could be expected.

Experimental Section

Synthesis. Starting materials for the preparation of $CaNiGe_2$, $SrNiGe_2$, and $SrNiSn_2$ were ingots of calcium and strontium (ChemPur), nickel wire (1 mm in diameter, Johnson-Matthey), tin tear drops (ChemPur), and germanium pieces (ChemPur), all with stated purities better than 99.9%. The calcium pieces were first arc-melted to form small buttons. The premelting procedure strongly reduces shattering of the calcium during the exothermic reaction with nickel and tin (or germanium). Pieces of calcium (or strontium), pieces of nickel wire, and pieces of germanium (or pieces of tin tear drops) were mixed in the ideal 1:1:2 atomic ratios and arc-melted. Each pellet was remolded three times, to ensure

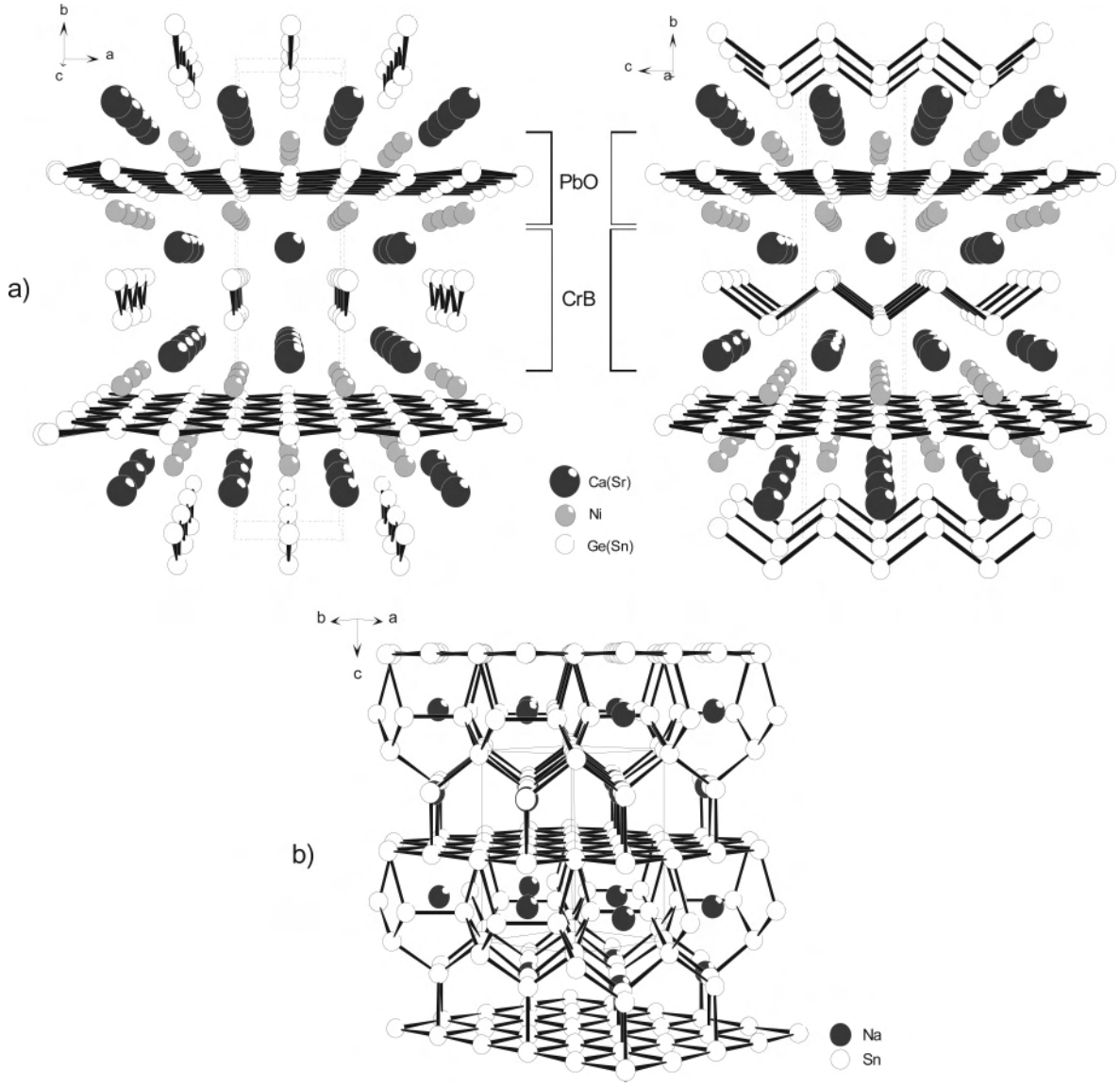

Figure 2. (a) Perspective view of the structure of $CaNiGe_2$, $SrNiGe_2$, and $SrNiSn_2$ along the *c*-axis (left-hand side) and the *a*-axis (right-hand side). (b) Schematic of the structure of $NaSn_5$.

homogeneity. The weight losses after the various melting procedures were always <0.5 wt %. All manipulations were performed in an argon-filled glove box.

After the melting procedures, only polycrystalline samples were obtained. For the growth of suitable single crystals for the structure determinations, a special heat treatment was used. The samples were crushed, powdered, and cold-pressed to pellets, then placed in tantalum containers and enclosed in evacuated silica tubes, which were placed in a muffle furnace. The samples were first heated to 1270 K within 6 h and held at that temperature for another 4 h. The temperature then was reduced at a rate of 6 K/h to 970 K, then at a rate of 24 K/h to 670 K, and finally cooled to room temperature within 3 h. After cooling to room temperature, the samples could easily be separated from the tantalum crucibles. No reactions of the samples with the crucible material could be detected. The polycrystalline samples are gray and stable against exposure to air and moisture. Single crystals exhibit a metallic luster.

X-ray Investigations. The purity of the samples was checked using a STOE STADI P powder diffractometer with Cu $K\alpha_1$ radiation. The orthorhombic lattice parameters (see Table 1) were obtained from least-squares fits of the powder data. The correct indexing was ensured through intensity calculations, taking the atomic positions from the structure refinements. In all cases, the lattice parameters determined from powder patterns and from single-crystal data agreed well with standard deviations (the 3σ rule). The powder diffractograms showed that, except for the main phase, the samples of $CaNiGe_2$ and $SrNiGe_2$ contained small amounts of the $CaNi_2Ge_2$, $SrNi_2Ge_2$, and unknown phases, whereas the sample of $SrNiSn_2$, except for the main phase, contained only minor amounts of elemental Sn.

Single-crystal intensity data for $SrNiGe_2$ and $SrNiSn_2$ were collected at room temperature, using a Stoe IPDS-IIT image plate diffractometer with graphite monochromatized Mo Kα (0.71073 Å) radiation in oscillation mode. Numerical absorption corrections were applied (X-Shape/X-Red).[31] The $CaNiGe_2$ crystal was measured at room temperature on an Oxford Xcalibur3 CCD area-detector diffractometer. All relevant crystallographic data for the data collections and refinement procedures are listed in Table 1.

(31) (a) X-RED (1.26)—Data Reduction Program. Stoe & Cie, Darmstadt, Germany, 2004. (b) X-SHAPE (2.05)—Crystal Optimization for Numerical Absorption Correction. Stoe & Cie, Darmstadt, Germany, 2004.

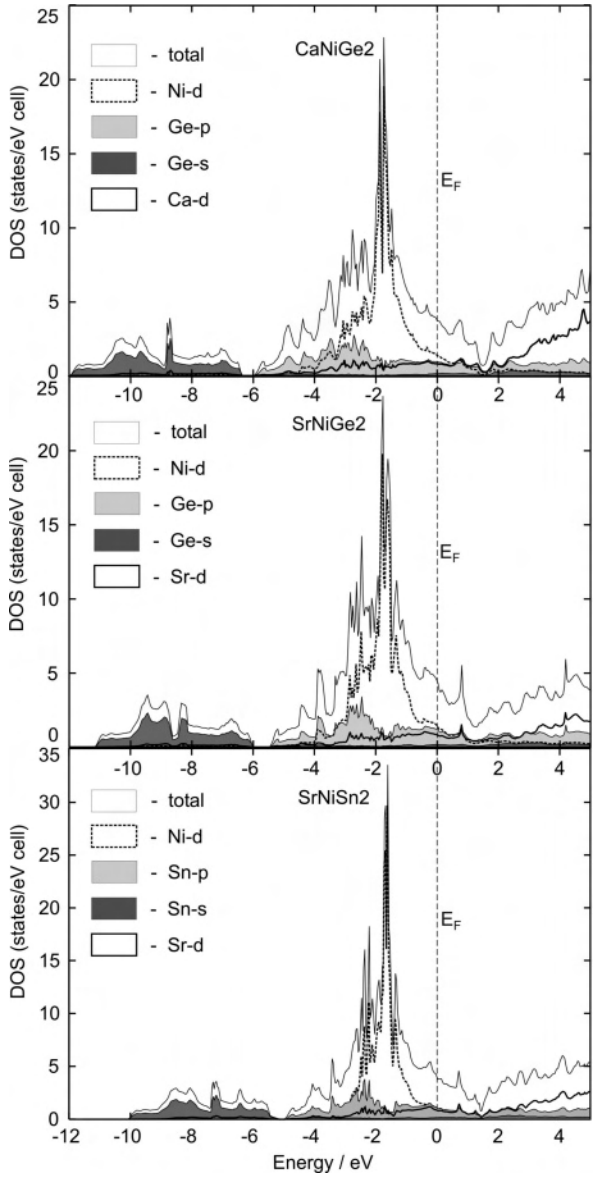

Figure 3. Total and projected density of states (DOS) curve for $CaNiGe_2$, $SrNiGe_2$, and $SrNiSn_2$. The energy zero is taken as the Fermi level.

Lattice parameters were determined from powder data and used for the refinement of the single-crystal data.

The single crystals used for the diffraction experiments were analyzed via scanning electron microscopy (JEOL model SEM 5900LV). The crystals were mounted on a sticky carbon disk that had been adhered to an aluminum holder and introduced into the SEM microscope. No impurities heavier than Na have been observed. Semiquantitative analyses of well-shaped single crystals revealed the following compositions (in atomic percentages): 27(2) Ca, 22(2) Ni, and 51(6) Ge for $CaNiGe_2$; 27(2) Sr, 22(2) Ni, and 54(6) Ge for $SrNiGe_2$; and 24(2) Sr, 23(3) Ni, and 53(4) Sn for $SrNiSn_2$. These values were in satisfactory agreement with the composition 1:1:2, obtained from the X-ray crystal structure analyses.

Electronic Structure Calculations. The electronic structures were calculated by means of the ab initio full-potential linear muffin-tin orbital (LMTO) methods in the atomic sphere approximation (ASA), using the tight-binding (TB) program TB-LMTO-ASA.[32] The analysis of the chemical bonding was based on theoretical density of states (DOS) curves, full-potential charge density plots, and crystal orbital Hamilton populations (COHPs).[33] COHP plots showed DOS curves, which were weighted by the contributions of each crystal orbital to some measure of the strength of a given bond. From COHP analyses, the contribution of the covalent part of a particular interaction to the total bonding energy of the crystal can be obtained. All COHP curves presented here are in a following format: positive values are bonding, and negative values are antibonding. The basis set of short-ranged[34] atom-centered TB-LMTOs contained s−f valence functions for Sr and Sn and s−d valence functions for Ca, Ni, and Ge. Ca 4p, Sr 5p and 4f, Ge 3d, and Sn 5d and 4f orbitals were included, using a down-folding technique.

Results and Discussion

Structure Refinements. Irregularly shaped single crystals of $CaNiGe_2$, $SrNiGe_2$, and $SrNiSn_2$ were isolated from the annealed samples by mechanical fragmentation. The crystal structures exhibit the Laue symmetry *mmm*, and the extinctions are consistent with space groups $Cmc2_1$ and *Cmcm*, which is the centrosymmetric version of which was determined to be the correct one during the structure refinements. The starting atomic parameters were obtained from an automatic interpretation of direct methods with SHELXS-97.[35] The structures were subsequently refined with anisotropic displacement for all atoms using SHELXL-97 (full-matrix least-squares on F^2).[36]

As a check for the correct composition and site assignment, the occupancy parameters were refined in separate series of least-squares cycles, along with the displacement parameters. All sites were determined to be fully occupied within two standard deviations (except for the Ni site in $SrNiSn_2$), and in the final cycles the full occupancies were used again. The occupancies of the Ni positions showed ∼98%. It is important to remember that the corresponding stannides of rare-earth metals form defect structure $RENi_{1-x}Sn_2$ with $x \leq 0.49$ (for RE = Ce).[8] Final difference Fourier syntheses revealed no significant residual peaks. The positional parameters and interatomic distances are listed in Tables 2 and 3.

Description of the Crystal Structures. The new intermetallic alkaline-earth compounds $CaNiGe_2$, $SrNiGe_2$, and $SrNiSn_2$ crystallize in the $CeNiSi_2$ structure.[7] The latter consists of a square pyramidal arrangement of $CeSi_2$ framework ($ZrSi_2$-type)[37] and intercalated transition-metal atoms. The trivalent Ce atoms is replaced by divalent Ca or Sr atoms, and the Si atoms by Ge or Sn atoms. The Ni atoms are located in the center of the pyramids (Figure 1).

(32) Van Schilfgarde, M.; Paxton, T. A.; Jepsen, O.; Andersen, O. K.; Krier, G. Programm TB-LMTO 4.6, Max-Planck-Institüt, Stuttgart, Germany, 1994.
(33) Dronskowski, R.; Blöchl, P. E. *J. Phys. Chem.* **1993**, *97*, 8617.
(34) Andersen, O. K.; Jepsen, O. *Phys. Rev. Lett.* **1984**, *53*, 2571.
(35) Sheldrick, G. M. SHELXS-97—Program for the Determination of Crystal Structures; University of Göttingen: Göttingen, Germany, 1997.
(36) Sheldrick, G. M. SHELXL-97—Program for Crystal Structure Refinement; University of Göttingen: Göttingen, Germany, 1997.
(37) Schachner, H.; Nowotny, H.; Kudielka, H. *Monatsh. Chem.* **1954**, *85*, 1140.

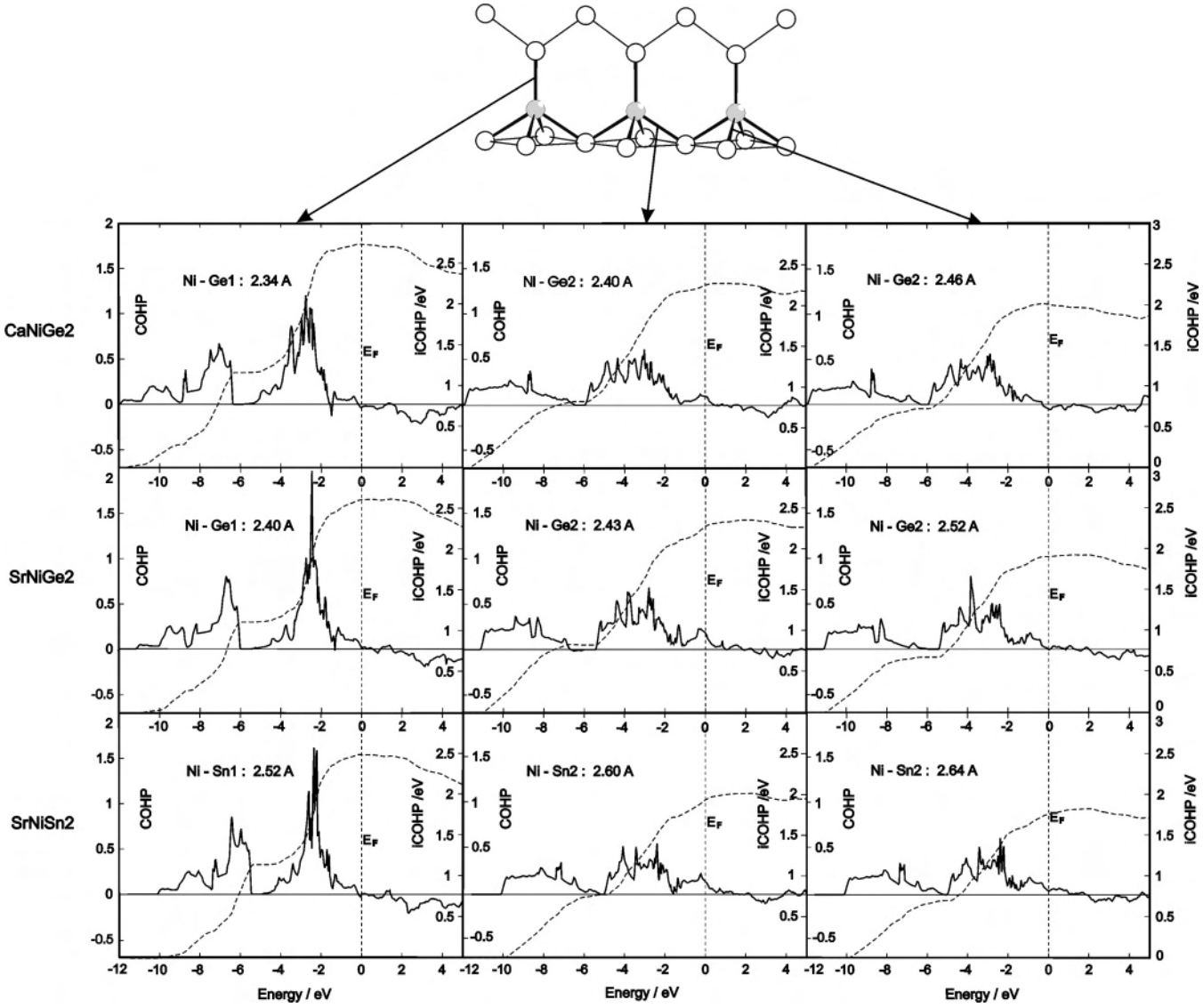

Figure 4. Crystal orbital Hamilton population (COHP) and integrated crystal orbital Hamilton population (iCOHP) curves for Ni−Ge(Sn) bonds within the NiX_5 pyramids.

The structure can also be described as an intergrowth of distorted slabs found in the crystals of CrB and PbO (Figure 2a), where the Ge1 or Sn1 atoms (X1) at the B positions form one-dimensional zig-zag chains running along the *c*-axis with X1−X1 distances of 2.50, 2.56, and 2.84 Å for $CaNiGe_2$, $SrNiGe_2$, and $SrNiSn_2$, respectively. These distances are slightly longer than the Ge−Ge distances in the elemental diamond-like Ge structure (2.45 Å) and the Sn−Sn distances in α-Sn (2.81 Å). Note that the Zintl phases CaGe, SrGe, and SrSn also adopt the CrB structure.[15,38] The Ge−Ge and Sn−Sn distances in CaGe, SrGe, and SrSn are 2.59, 2.63, and 2.94 Å, and thus longer than those in the structures of the title compounds, indicating stronger X1−X1 bonding in the zig-zag chains of $CaNiGe_2$, $SrNiGe_2$, and $SrNiSn_2$. In the structures of $CaNiGe_2$, $SrNiGe_2$, and $SrNiSn_2$ the Ge2(Sn2) atoms form quadratic layers, with the Ni atoms capping the centers of the squares (Figure 2a). The Ge2−Ge2 and Sn2−Sn2 distances (2.93, 3.05, and 3.22 Å in $CaNiGe_2$, $SrNiGe_2$, and $SrNiSn_2$, respectively) are much longer than those in elemental Ge and β-Sn. In $NaSn_5$,[39] which contains the same distorted quadratical Sn-network (Figure 2b), the corresponding Sn2−Sn2 contacts are slightly shorter than those in $SrNiSn_2$.

The Ni atoms in $CaNiGe_2$, $SrNiGe_2$, and $SrNiSn_2$ are surrounded by five Ge (Sn) neighbors, in the form of distorted square pyramids. The Ni−Ge and Ni−Sn distances are in the range of 2.34−2.46, 2.40−2.52, and 2.52−2.64 Å, respectively, with the longest distances being those extending to the Sn atoms at the top of pyramids. These distances agree well with the sum of the covalent radii of 2.45 Å ($r_{Ni} + r_{Ge}$) and 2.64 Å ($r_{Ni} + r_{Sn}$),[40] indicating strong Ni−X interactions.

The Ni-centered X_5 pyramids are condensed via common edges, thereby generating two-dimensional layers parallel to the *ac* plane, with the tops of the pyramids of adjacent layers

(38) Becker, D.; Beck, H. P. *Z. Kristallogr.* **2004**, *219*, 348.

(39) Fässler, T. F.; Kronsender, C. *Angew. Chem., Int. Ed. Engl.* **1998**, *37* (11), 1571.

(40) Pauling, L.; Kamb, B. *Proc. Natl. Acad. Sci. (USA)* **1986**, *83*, 3569.

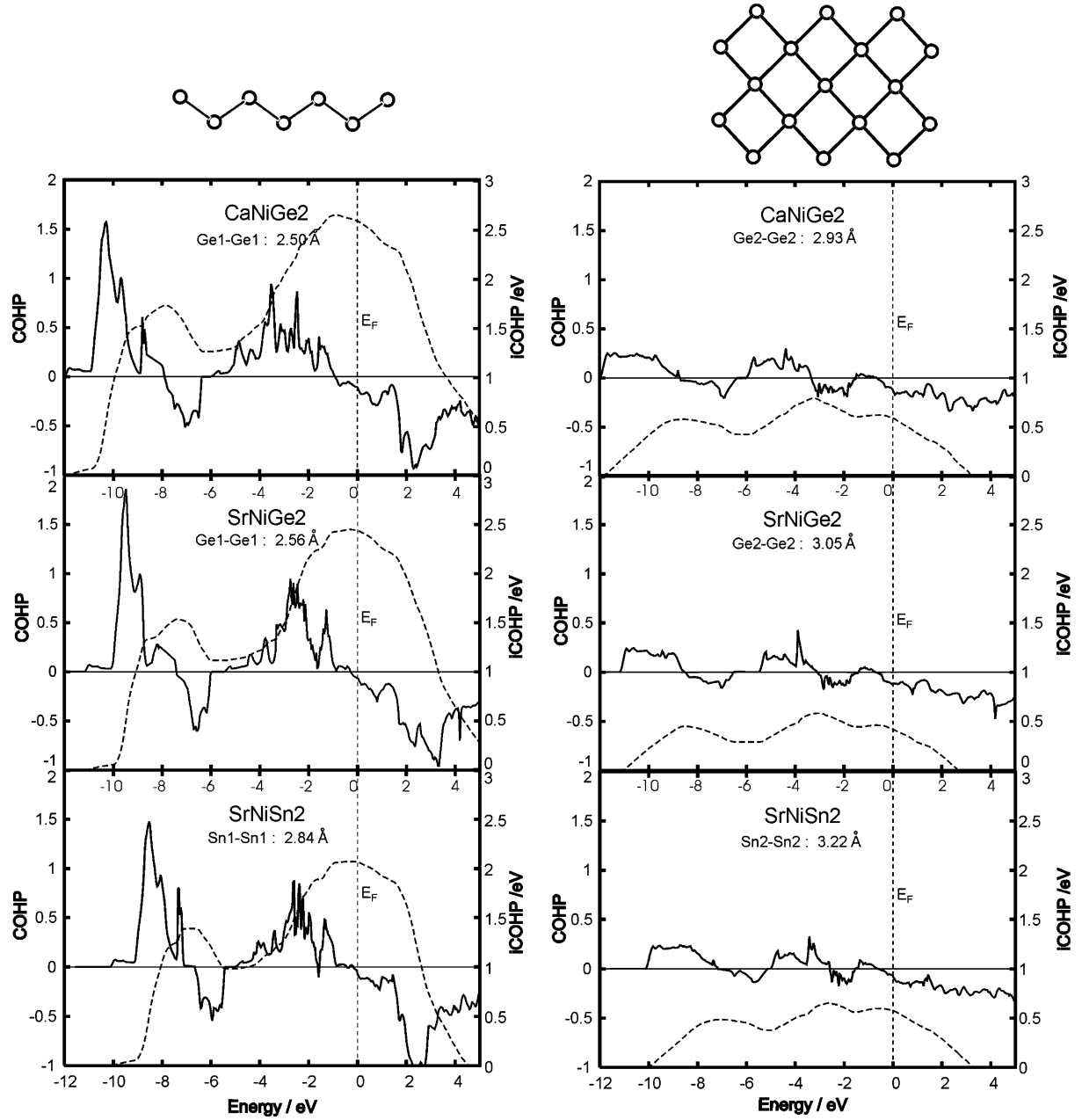

Figure 5. COHP and iCOHP curves for the Ge1−Ge1 and Sn1−Sn1 bonds in the Ge and Sn zig-zag chains, and the Ge2−Ge2 and Sn2−Sn2 contacts within the Ge or Sn squares of $CaNiGe_2$, $SrNiGe_2$, and $SrNiSn_2$.

forming Ge1(Sn1) zig-zag chains (Figure 1) along the *c*-direction. This arrangement of the Ni and Ge (Sn) atoms leads to a three-dimensional network without any Ni−Ni contacts, in which the Ca (Sr) atoms fill distorted channels.

The Ca−Ni and Sr−Ni contacts in $CaNiGe_2$, $SrNiGe_2$, and $SrNiSn_2$ (3.16, 3.30, and 3.49 Å) are significantly longer than the sum of Pauling's single-bond radii of 2.98 Å ($r_{Ca} + r_{Ni}$) and 3.15 Å ($r_{Sr} + r_{Ni}$), whereas the shortest Ca−Ge, Sr−Ge, and Sr−Sn contacts (3.18, 3.24, 3.48 Å) are also longer than the corresponding Pauling radii (2.98 Å ($r_{Ca} + r_{Ge}$), 3.16 Å ($r_{Sr} + r_{Ge}$) and 3.35 Å ($r_{Sr} + r_{Sn}$)).[40]

Chemical Bonding. The nature of the chemical bonding in $CaNiGe_2$, $SrNiGe_2$, and $SrNiSn_2$ was investigated by TB-LMTO-ASA[32] band structure calculations. The corresponding total and partial DOS plots are shown in Figure 3. In all cases, the Fermi level is ~1.5 eV below a pseudo-gap, which is very pronounced in $CaNiGe_2$ and $SrNiSn_2$. In the valence region, the DOS has significant nickel d-character; the profile of the projected DOS between −4.5 eV up to the Fermi level shows their mixing with Ge(Sn)-p, and partially Ca(Sr)-d states. The states below −6 eV originate essentially from Ge (or Sn) s-orbitals.

To obtain a quantitative measure of the bond strengths, COHPs were determined.[33] Each of the COHP curves and integration values represent a weighted average of multiple (similar) bonds, thereby allowing a direct comparison of their strengths. The strongest bonding interaction occurs for the three shortest Ni−Ge or Ni−Sn contacts within the NiX_5 pyramids (Figure 4). The Fermi level separates the bonding and antibonding Ni−Ge or Ni−Sn interactions.

The Ge1−Ge1 and Sn1−Sn1 bonds within the zig-zag chains are much stronger than those within the Ge2 and Sn2

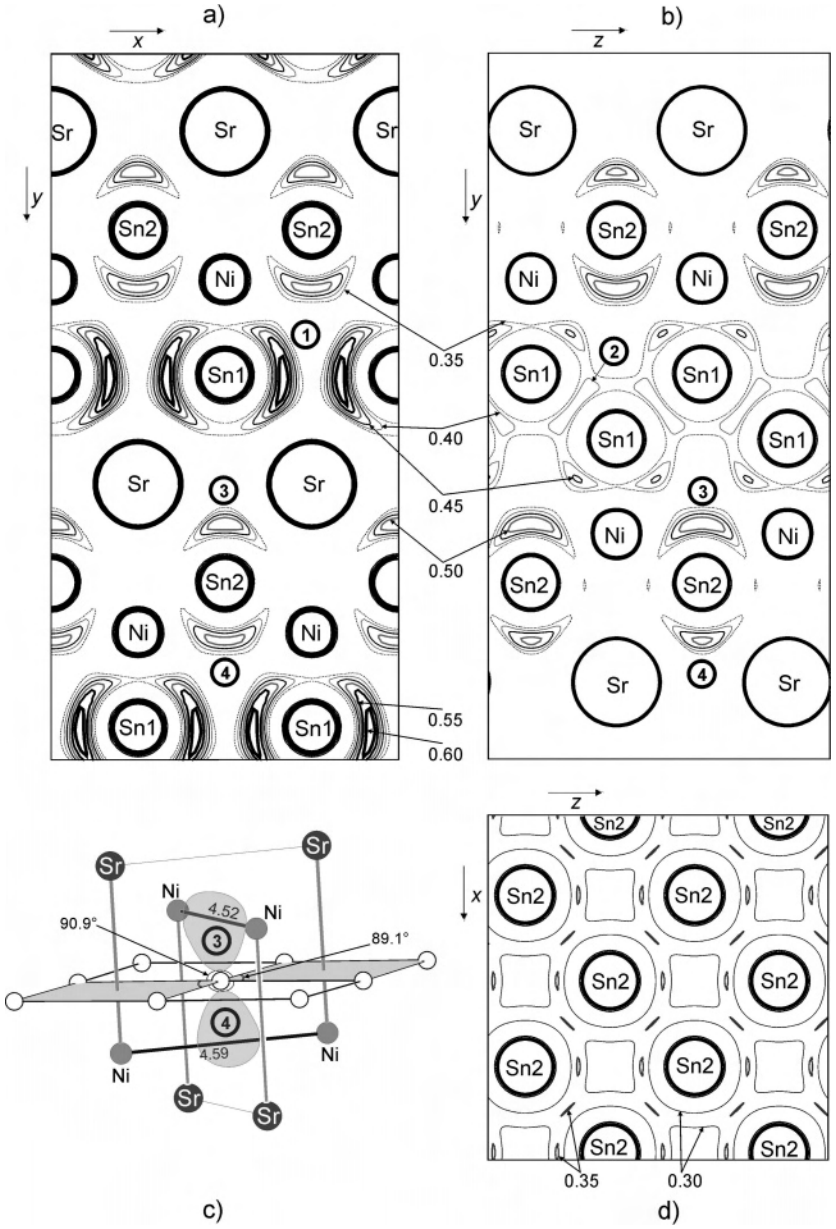

Figure 6. Contour line diagrams of the all-electron electron localization function (ELF) in progressive steps of 0.05 for $SrNiSn_2$: (a) *xy* plane at $z = 0.25$; (b) *yz* plane at $a = 0$; (c) schematic drawing of the lone pair regions at the Sn2 atoms; (d) *xz* plane at $y = 0.25058$.

squares (Figure 5), which is in agreement with the longer interatomic distances within the squares. In the Zintl phases CaGe, SrGe, and SrSn, the integrated COHP values of the corresponding Ge−Ge or Sn−Sn bonds within the zig-zag chains[38] are smaller than those calculated for $CaNiGe_2$, $SrNiGe_2$, and $SrNiSn_2$. This is in agreement with longer distances in the 1:1 phases. As expected, the Ca−Ni and Sr−Ni and the Ca−Ge, Sr−Ge, and Sr−Sn interactions are observed to be very weak.

For a deeper insight into the nature of the chemical bonding, band structure analyses that apply the Electron Localization Function (ELF) were performed.[41−44] For the localization of the Sn−Sn bonding and nonbonding electrons in $SrNiSn_2$, the function is represented in Figure 6 parallel to the *xy*, *yz* (section of the Sn1 zig-zag chains), and *xz* planes (section of the quadratic layers of Sn2). ELF values are defined between 0 and 1. ELF maxima in the region of the atom cores are attributed to various shells and, in the region of the valence electrons, either to covalent bonds or to lone pairs of electrons. The ELF map in Figure 6 renders contour lines with an increment of 0.05.

Figure 6a shows the contour diagram of the ELF topology of $SrNiSn_2$ in the *xy* plane at $z = 0.25$. The Sn1 chains are oriented perpendicular to the picture along the *c*-axis. At each Sn1 atom of the zig-zag chain, two lone pairs (identified by the symbol "①") with their orientation perpendicular to the plane of the zig-zag chain become visible, with ELF values of >0.6. This valence electron localization domain includes

(41) Becke, A. D.; Edgecomb, K. E. *J. Chem. Phys.* **1990**, *92*, 5397.
(42) Savin, A.; Nesper, R.; Wengert, S.; Fässler, T. F. *Angew. Chem., Int. Ed. Engl.* **1997**, *36*, 1809−1832.
(43) Fässler, T. F.; Savin, A. *Chem. Unserer Zeit* **1997**, *31*, 110.
(44) Fässler, T. F. *Chem. Soc. Rev.* **2003**, *32*, 80.

the highest ELF value observed for $SrNiSn_2$ and resembles lone pairs with p_z-orbital character. The bonding region between two adjacent Sn1 atoms within the chains (identified by the symbol "②") is shown in Figure 5b, which reflects a contour line diagram of the ELF topology in the *yz* plane at $x = 0$. ELF maxima with values of ~0.4 are located between neighboring Sn1 atoms, which can be interpreted as localized covalent Sn−Sn bonds. There are no attractors between the Sn1 and Ni atoms.

Figure 6a,b clearly reveals nonbonding electron pair domains with ELF values of >0.5 at Sn2 atoms located above (identified by the symbol "③") and below (identified by the symbol "④") the Sn2 squares. The nonbonding electron pairs are oriented along the *y*-axis and resemble p_y-orbital character. The Sn squares of the network are alternately capped by Ni and Sr atoms above and below the plane, with the Sr and the Ni caps opposing each other (see Figure 6c). The lone pairs at Sn2 are located in a cavity built by the Sn atom, two Sr atoms, and two Ni atoms. Because of the slight distortion of the squares (orthorhombic instead of tetragonal symmetry), the diagonal Ni−Ni distances above and below the plane are different (see Figure 6a and b). The lone-pair domain marked "③" is larger in the region of shorter Ni−Ni (4.52 Å) and longer Sr−Sr contacts (4.59 Å) and vice versa.

Figure 6d shows an ELF section parallel to the quadratic Sn2 network in the *xz* plane at $y = 0.25058$. ELF maxima between adjacent Sn atoms appear only at low values (~0.35) and indicate small covalent contributions to the bonding between these atoms, which is in agreement with results obtained for other intermetallic compounds with similar Sn−Sn distances.[5]

Conclusion

The intermetallic compounds $CaNiGe_2$, $SrNiGe_2$, and $SrNiSn_2$ combine structural motifs that are known from Ge and Sn substructures of binary phases without transition metals. The observed Ge and Sn zig-zag chains with covalent interactions are also observed in the binary Zintl phases (AE)-Ge and (AE)Sn (where AE = Ca, Sr, Ba), and more-or-less distorted quadratic networks of Sn atoms with metallic bonding are encountered in $SrSn_4$. Both bonding characteristics are also present in the novel phases. In both $SrSn_4$ and $NaSn_5$, localized and delocalized bonding are observed. The present study shows that this feature also is retained in transition-metal-containing phases. However, the bond analyses of the title compounds are not straightforward, because, according to atomic distance considerations, the Ni−Ge and Ni−Sn interactions seem to be of a covalent nature. On the other hand, the bond analyses of the stannide, by electron localization function (ELF) calculations, reveal no attractors between the Ni and Sn atoms.

In analogy to the situation encountered in the CrB-type structures, strong covalent interactions between the atoms of the zig-zag chains appear. Further, lone pairs perpendicular to the plane of the zig-zag chains occur. In the title compounds, lone pairs at the Sn atoms of the quadratic net are observed with their orientation perpendicular to the plane of the net. This bond situation is also observed in $NaSn_5$, where only one lone pair is located at each Sn atom of the quadratic network with an orientation alternatively above and below the plane, whereas each Sn atom in $SrNiSn_2$ carries two lone pairs, pointing toward both sides of the plane. Considering the close relationship between bonding and nonbonding electrons in the sense of the valence-shell electron-pair repulsion model, both quadratic networks in $NaSn_5$ and $SrNiSn_2$ are rather similar, with respect to the localized part of chemical bonding. As in binary Ni−Sn compounds, the Ni−Sn distances in $SrNiSn_2$ are rather short, and there are no indications for covalent bonding between these atoms, according to the results of the ELF calculations.

Acknowledgment. The authors thank the Bayerische Forschungsstiftung for financial support. The authors would like to thank Dr. Annette Schier for her help with the correction of the manuscript.

Supporting Information Available: X-ray crystallographic files (CIF format). This material is available free of charge via the Internet at http://pubs.acs.org.

IC060613Y